Temporal Control of Self-Oscillation for Microgels by Cross-Linking Network Structure

Daisuke Suzuki[†] and Ryo Yoshida*[,†,‡]

Department of Materials Engineering, Graduate School of Engineering, The University of Tokyo, 7-3-1 Hongo, Bunkyo-ku, Tokyo 113-8656, Japan, and PRESTO, Japan Science and Technology Agency, 4-1-8 Honcho Kawaguchi, Saitama, Japan

Received March 28, 2008; Revised Manuscript Received June 3, 2008

ABSTRACT: Self-oscillating microgel, which undergoes an autonomic and periodical swelling/deswelling oscillation, has been reported. The cross-linked microgels were synthesized by the copolymerization of *N*-isopropylacrylamide (NIPAm) with ruthenium tris(2,2′-bipyridine) [$Ru(bpy)_3$] as a catalyst for the Belousov−Zhabotinsky (BZ) reaction by surfactant-free aqueous precipitation polymerization. The self-oscillation of the microgels was detected by changes in optical transmittance. The microgels showed not only the swelling/deswelling oscillation, which is synchronized with the redox oscillation of the $Ru(bpy)_3$ complex immobilized in the microgels, but also flocculating/dispersing oscillation around the phase transition temperature of the microgels, with a remarkable change in optical transmittance. These microgel oscillations were further studied by comparing the optical transmittance changes of the microgels and the redox potential change of $Ru(bpy)_3$ immobilized in the microgels. In order to analyze the microgel self-oscillation in detail, three characteristics (induction period, oscillation period, and waveform) of the microgel oscillation were compared with those of the bulk solution of the BZ reaction. Because of the effect of $Ru(bpy)_3$ immobilization in the microgels on the BZ reaction, induction time for the microgels became longer than that for the bulk solution; however, the oscillation periods became shorter. The latter can be well explained by the Field−Körös−Noyes (FKN) mechanism.

Introduction

Microgels composed of stimulus-responsive polymers have attracted much attention due to their potential applications in many fields, such as drug delivery,[1,2] microreactors,[3−5] chemical/biological separations,[6] emulsifiers,[7,8] photonic crystals,[9−12] and microlenses.[13] One of the most widely studied stimulus-responsive microgels is composed of poly(*N*-isopropylacrylamide), pNIPAm, which is a thermoresponsive polymer with a lower critical solution temperature (LCST) of about 31 °C in pure water.[14,15] Microgels of pNIPAm have a volume phase transition temperature (VPTT) around the LCST of pNIPAm, and various functional groups have been added by copolymerization or postpolymerization modification to make the gel multiresponsive (e.g., temperature and other factors such as pH,[16] light,[17] presence of biomolecules,[18] and so on). These microgels change their properties when on/off switching of external stimuli occurs.

In contrast to the stimulus-responsive microgels, recently, we have developed "self-oscillating" microgels that undergo an autonomic and periodical swelling/deswelling oscillation without any external stimulus by copolymerizing ruthenium tris(2,2′-bipyridine), denoted $Ru(bpy)_3$, into a cross-linked pNIPAm microgel.[19] $Ru(bpy)_3$ was selected as a catalyst for the Belousov−Zhabotinsky (BZ) reaction,[20] which generates rhythmical redox changes from the oxidized Ru^{III} state to the reduced Ru^{II} state. When the microgels were dispersed in an aqueous acidic solution containing the substrates for the BZ reaction (such as malonic acid, sodium bromate), periodical swelling/deswelling oscillation of each microgel is spontaneously induced by the BZ reaction occurring in the microgel.

Up to now, our group has created "self-walking" actuators using millimeter size self-oscillating gel,[21] which may be useful as artificial muscles. Besides, self-oscillating macro (bulk) gel would have potential applications such as pumps with autonomous beating, oscillatory drug release synchronized with cell cycles, or human biorhythms.[22] Other than these potential applications, self-oscillating microgels that disperse in aqueous medium would be useful as artificial oscillators, rheological modifiers, light-modulating liquid, and so on. Moreover, volume oscillation of microgels might regulate microgel assembly by controlling interparticle interactions. Actually, we have already found that volume oscillation led to change interparticle interactions, which resulted in self-dispersing/self-flocculating oscillation of microgels.[19] To achieve these applications of self-oscillating microgels, it should be important to understand how self-oscillation of microgels can be controlled.

In this paper, we present the synthesis and characterization of self-oscillating microgels in detail. Self-oscillating microgels were synthesized using NIPAm, $Ru(bpy)_3$ monomer, and *N,N*′-methylenebis(acrylamide) (BIS) cross-linker by surfactant-free aqueous precipitation polymerization as previously reported.[19] Here, the effects of $Ru(bpy)_3$ monomer and cross-linker amount on microgel formation by precipitation polymerization are presented as well as self-oscillation study using obtained microgels. The volume oscillation of the microgels was detected by changes in optical transmittance. In order to analyze the self-oscillation profiles of microgels, three characteristics (i.e., induction period, oscillation period, and waveform) of the microgel self-oscillation were compared with those of the bulk solution of the BZ reaction as a control. In particular, self-flocculating/self-dispersing oscillation,[19] which is observed around the phase transition temperature of the microgels, was examined by comparing transmittance changes of microgel oscillation with redox potential changes of the $Ru(bpy)_3$ complex. Through the analysis of microgel self-oscillation, effect of catalyst immobilization in microgels on the BZ reaction was discussed.

Experimental Details

Materials. Unless stated otherwise, all reagents were purchased from Wako Pure Chemical Industries, Ltd. *N*-Isopropylacrylamide

* To whom correspondence should be addressed. E-mail: ryo@cross.t.u-tokyo.ac.jp.
† The University of Tokyo.
‡ PRESTO, Japan Science and Technology Agency.

10.1021/ma800684d CCC: $40.75
Published on Web 07/08/2008

(NIPAm, Sigma-Aldrich) was recrystallized from hexanes and dried in vacuo prior to use. The cross-linker *N,N′*-methylenebis(acrylamide) (BIS, Kanto Chemical Co., Inc.) and the initiator azobis(amidinopropane) dihydrochloride (V-50) were used as received. Ruthenium(II) (4-vinyl-4′-methyl-2,2′-bipyridine)bis(2,2′-bipyridine)bis(hexafluorophosphate) [$Ru(bpy)_3$ monomer] was synthesized according to the previous work.[22,23] Malonic acid (MA), sodium bromate ($NaBrO_3$, Kanto Chemical Co., Inc.), nitric acid (HNO_3, Kanto Chemical Co., Inc.), cerium(IV) sulfate tetrahydrate [$Ce(SO_4)_2 \cdot 4H_2O$], cerium(III) sulfate *n*-hydrate ($n = 5$) [$Ce_2(SO_4)_3 \cdot 5H_2O$], and sodium chloride (NaCl) were all used as received. Water for all reactions, solution preparation, and polymer purification was first distilled and then ion-exchanged.

Microgel Synthesis. The $Ru(bpy)_3$ copolymerized pNIPAm microgels were synthesized via surfactant-free aqueous radical precipitation polymerization as previously reported.[19] A mixture of NIPAm, $Ru(bpy)_3$, BIS, and water (95 mL) was poured into a 200 mL three-neck, round-bottom flask equipped with a stirrer, a condenser, and a nitrogen gas inlet. The initial total monomer concentration was held constant at 150 mM, and the comonomer ratio, $(1-X-Y:X:Y)$ (NIPAm:$Ru(bpy)_3$:BIS), was varied according to the desired $Ru(bpy)_3$ monomer and cross-linker concentration. Under a stream of nitrogen to purge oxygen and with constant stirring, the solution was heated in an oil bath to 70 °C. After stabilizing the solution for 1 h, the V-50 initiator (0.054 g) dissolved in 5 mL of water was added to the flask to start the polymerization, which then continued for 6 h. After polymerization, the dispersion was cooled to room temperature. The obtained microgels were purified by centrifugation/redispersion with water four times using a relative centrifugal force (RCF) of 52490*g* and by daily changes of water by means of dialysis for a week. The obtained microgels were denoted as NRu*X*(*Y*). In the sample code, N and Ru stand for NIPAm and $Ru(bpy)_3$, respectively, while the number following each letter represents the mole percentage of $Ru(bpy)_3$ fed in polymerization. After the number, the mole percentage of BIS fed in polymerization is shown in parentheses.

Characterization. Microgel sizes and polydispersity indices (PDI) were determined by dynamic light scattering (DLS, Malvern, Zetasizer3000HS_A). PDI values were calculated from the cumulants analysis as defined in ISO13321.[24,25] Diluted microgels were analyzed in a quartz cuvette (microgel concentration: 0.005 wt %). The samples were allowed to equilibrate at the desired temperature for 10 min before data collection. Scattered light was collected at 90°. NaCl was then used to adjust each solution to 1 or 10 mM total ion concentration. Moreover, in order to maintain the reduced Ru^{II} and oxidized Ru^{III} states, 1 mM Ce^{III} and 0.3 M HNO_3 solution and 1 mM Ce^{IV} and 0.3 M HNO_3 solution were used, respectively.

The amount of introduced $Ru(bpy)_3$ into the microgels was calculated on the basis of UV−vis measurements (Shimadzu UV-2500PC). Absorbance at 460 nm, which is a wavelength of the maximum absorbance for $[Ru(bpy)_3]^{2+}$, of the microgels dispersed in pure water was determined to calculate the introduced $Ru(bpy)_3$ monomer into the microgels.

Optical transmittance data of oscillations were collected on a Shimadzu UV-2500PC spectrophotometer. Before the self-oscillation study, transmittance changes as a function of temperature for the reduced Ru^{II} and oxidized Ru^{III} states at high salt concentrations were collected. Microgels (0.1 wt %) were dispersed in 1 mM Ce^{III} and 0.3 M HNO_3 solution or in 1 mM Ce^{IV} and 0.3 M HNO_3 solution to maintain the reduced Ru^{II} and oxidized Ru^{III} states, respectively. The measurements were taken at a heating rate of 1 °C/min from 20 to 40 °C under constant stirring. For the self-oscillation study, microgels were dispersed in aqueous solution containing the reactants of the BZ reaction: MA (62.5 mM), $NaBrO_3$ (84 mM), and HNO_3 (0.3 M). Under constant temperature and stirring conditions, the time course of transmission was monitored. The $Ru(bpy)_3$ complex has different absorption spectra in the reduced Ru^{II} state and the oxidized Ru^{III} state as an inherent property. The solution exhibited the absorption maximum at ∼460 nm in the reduced state and at ∼420 nm in the oxidized state and has an isosbestic point at 570 nm. In this study, the 570 nm wavelength was selected to detect the swelling/deswelling signals of microgels while the 460 nm wavelength was used to detect the redox change of $Ru(bpy)_3$ for the bulk solution of the BZ reaction as a control (see Supporting Information).

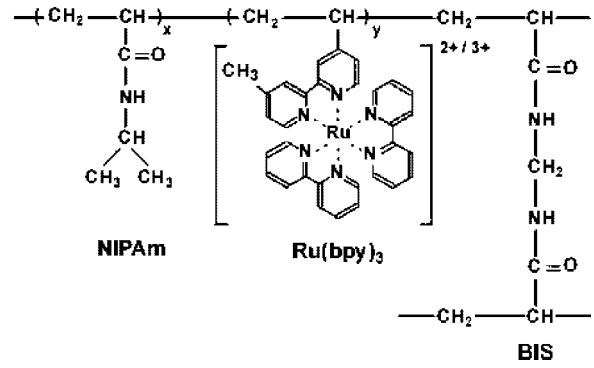

Figure 1. Chemical structure of the microgel.

Electrochemical measurements were performed simultaneously with optical transmittance measurements to check the synchronization between the redox oscillation of $Ru(bpy)_3$ complex and the mechanical oscillation of the microgel.[26] Redox potential changes were monitored using potentiometer (Hokuto Denko, HA-150G) with Pt electrodes.

Results and Discussion

Microgel Synthesis. The synthesis of the self-oscillating microgels was carried out using NIPAm, $Ru(bpy)_3$ monomer, and BIS cross-linker through surfactant-free aqueous precipitation polymerization as described in our previous paper.[19] The chemical structure of the microgel is shown in Figure 1. This is a conventional method for preparing pNIPAm microgels, as the monomer is soluble under the reaction conditions, but the polymer undergoes a phase separation into globules.[15,27] Herein, in order to clarify the effect of $Ru(bpy)_3$ monomer on the microgels, the polymerization was conducted by varying the fed $Ru(bpy)_3$ monomer amount. Note that the $Ru(bpy)_3$ moieties were fixed in the reduced Ru^{II} state in polymerization and characterization. Table 1 shows the $Ru(bpy)_3$ introduced amounts and the microgel sizes under the different temperatures (25 and 55 °C, which is below and above pNIPAm LCST, respectively) and salt concentrations. $Ru(bpy)_3$ were introduced in microgels ∼50−60% for all samples. PDI indices were below 0.16 for all batches of $Ru(bpy)_3$ immobilized microgels at all conditions, indicating that the polymerization was not perturbed by $Ru(bpy)_3$ groups. In 1 mM NaCl solution, microgel sizes at 25 °C, where the microgels were highly swollen, became smaller as fed $Ru(bpy)_3$ monomer increased. This tendency was also seen at 55 °C, where the microgels were deswollen. These results suggest that $Ru(bpy)_3$ monomer plays as stabilizers of the precursor particles in precipitation polymerization; thus, the aggregation of the precursor particles was suppressed in the early stage, and microgel sizes became smaller. This effect may be similar to that of ionic surfactants in precipitation polymerization.[15,28] But the NRu1(1) microgels show larger sizes both at 25 and 55 °C than those having less $Ru(bpy)_3$ monomer [i.e., NRu0.5(1) microgels]. This may be due to the electrostatic repulsion of $Ru(bpy)_3$ immobilized in pNIPAm chains;[29] thus, the NRu1(1) swells more than the other microgels at the constant temperature. The size in 10 mM NaCl solution at 55 °C shows another characteristic of $Ru(bpy)_3$-immobilized microgels. Microgels having less $Ru(bpy)_3$ monomer [i.e., NRu0(1)−NRu0.1(1) microgels] flocculated under the condition while the others [i.e., NRu0.2(1)−NRu1(1) microgels] did not. This indicates that $Ru(bpy)_3$ groups in microgels stabilizes the microgels. Table 1 also shows impact of BIS cross-linker concentration on the sizes.

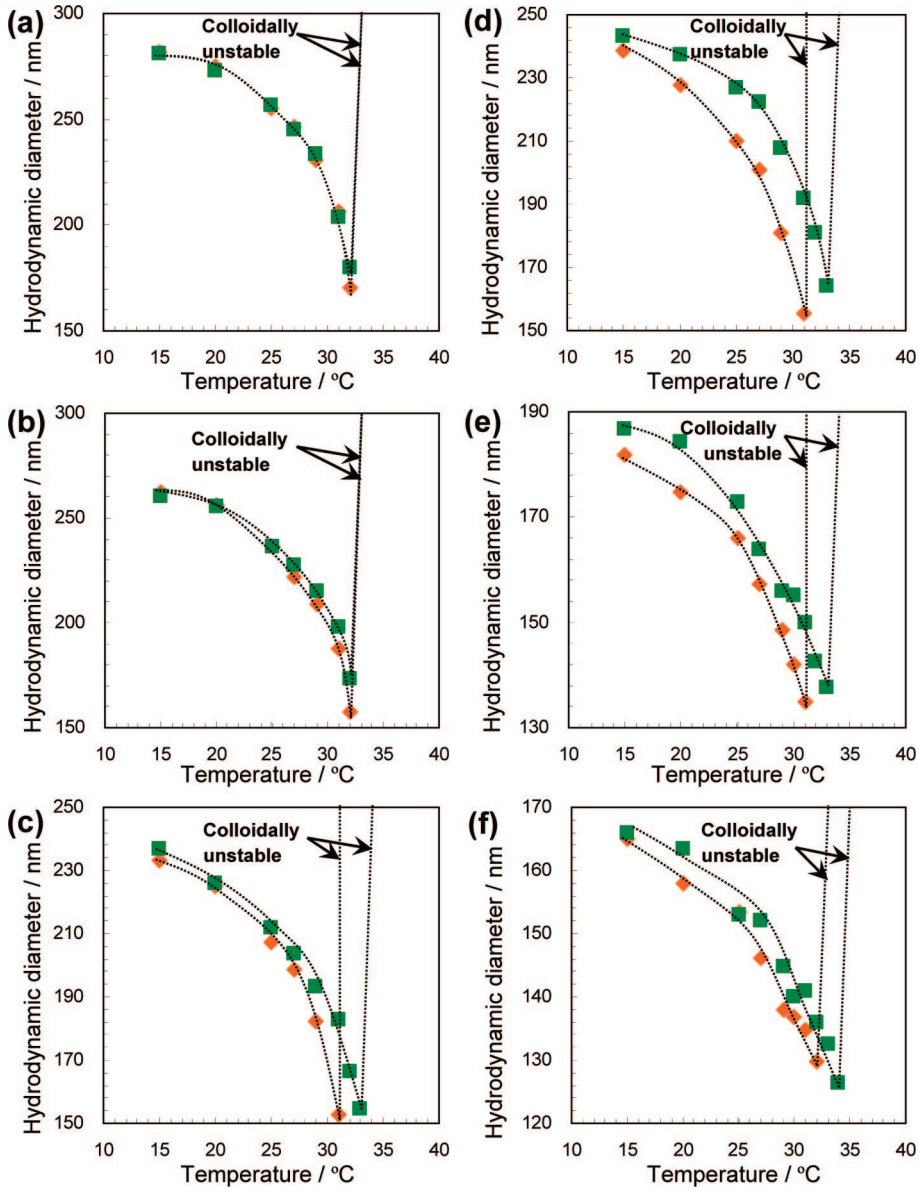

Figure 2. Deswelling curves for the $Ru(bpy)_3$ copolymerized pNIPAm microgels under the different conditions, as measured by dynamic light scattering: the reduced state Ru^{II} in 1 mM Ce^{III} and 0.3 M HNO_3 solution (orange diamond) and the oxidized state Ru^{III} in 1 mM Ce^{IV} and 0.3 M HNO_3 solution (green square). Samples are (a) NRu0.1(1), (b) NRu0.2(1), (c) NRu0.5(1), (d) NRu1(1), (e) NRu1(4), and (f) NRu1(10) microgels. The dispersion concentration was 0.005 wt % in all cases.

Table 1. Microgel Sizes under Different Conditions

			1 mM NaCl				10 mM NaCl	
	$Ru(bpy)_3$ amount, mol %		25 °C		55 °C		55 °C	
sample[a]	fed	introduced	D, nm[b]	PDI[b]	D, nm[b]	PDI[b]	D, nm[b]	PDI[b]
NRu0(1)	0		860	0.287	360	0.026	1155[c]	
NRu0.01(1)	0.01	N.A.	476	0.074	189	0.006	1181[c]	
NRu0.05(1)	0.05	0.05	337	0.007	128	0.013	472[c]	
NRu0.1(1)	0.1	0.07	275	0.062	104	0.045	155[c]	
NRu0.2(1)	0.2	0.12	252	0.043	96	0.019	95	0.047
NRu0.5(1)	0.5	0.34	249	0.150	108	0.050	88	0.077
NRu1(1)	1	0.56	291	0.159	167	0.056	129	0.125
NRu1(4)	1	0.47	202	0.046	128	0.003	105	0.009
NRu1(10)	1	0.50	167	0.011	109	0.008	100	0.034

[a] In the sample code, N and Ru stand for NIPAm and $Ru(bpy)_3$, respectively, while the number following each letter represents the mole percentage of $Ru(bpy)_3$ fed in polymerization. After the number, the mole percentage of BIS fed in polymerization is shown in parentheses. [b] D denotes hydrodynamic diameters of microgels, and PDI is polydispersity index. All samples were allowed to equilibrate at the certain temperature for 10 min before data collection. [c] Microgels are flocculated under the conditions The size of microgel aggregates changed during the measurements.

As increasing the BIS amount fed in polymerization, the microgel sizes at the swollen state became smaller, which is reasonable because highly cross-linked hydrogel is restricted to swell.

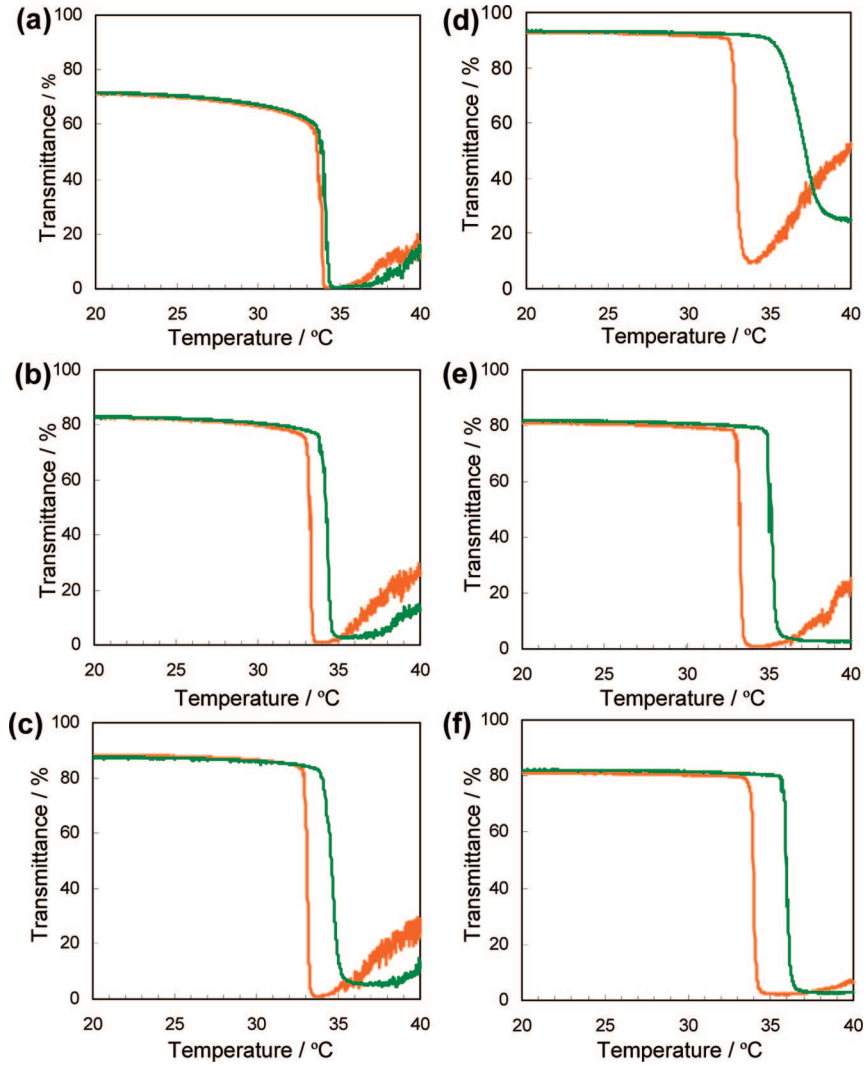

Figure 3. Temperature dependence of optical transmittance for the $Ru(bpy)_3$ copolymerized pNIPAm microgels under the different conditions of the reduced state Ru^{II} in 1 mM Ce^{III} and 0.3 M HNO_3 solution (orange line) and the oxidized state Ru^{III} in 1 mM Ce^{IV} and 0.3 M HNO_3 solution (green line). Samples are (a) NRu0.1(1), (b) NRu0.2(1), (c) NRu0.5(1), (d) NRu1(1), (e) NRu1(4), and (f) NRu1(10) microgels. The dispersion concentration was 0.1 wt % in all cases. The 570 nm wavelength was used for the measurement. The solutions were heated at a rate of 1 °C/min.

Microgel Properties Both in the Ru^{II} and the Ru^{III} States. Before the self-oscillation study, we checked the changes of microgel properties between in the reduced Ru^{II} and the oxidized Ru^{III} states. First, hydrodynamic diameters of NRu microgels were determined as a function of temperature in the reduced Ru^{II} and the oxidized Ru^{III} states by DLS. Herein, each solution contains 0.3 M HNO_3 because the BZ reaction only occurs at high salt concentrations (greater than 0.3 M). As can be seen from Figure 2a, for NRu0.1(1) microgels, there is little difference of the diameters between in the Ru^{II} and the Ru^{III} states at the same temperatures. Note that the size of microgel aggregates changed as a function of time. In addition, the microgels were flocculated at 33 °C in both the Ru^{II} and the Ru^{III} states. In general, pNIPAm microgels in pure water are colloidally stable both below and above the VPTT. Particularly, above the VPTT, pNIPAm microgels are colloidally stable due to electrostatic repulsion from the residues of initiator although steric hindrance is not so effective. Here NRu0.1(1) microgels were flocculated at 33 °C (= critical flocculation temperature, denoted CFT) because interparticle electrostatic repulsion is greatly reduced due to high salt concentration. However, in contrast to hard particles such as polystyrene and silica particles, the flocculated microgels could be redispersed when cooled quickly below the VPTT. Next, increase of $Ru(bpy)_3$ amount in microgels led to increase not only in size deviation between the Ru^{II} and the Ru^{III} states at the same temperatures but also in CFT's differences between in the Ru^{II} and Ru^{III} states as shown in Figure 2b−f. These CFT shifts are due to increased hydrophilicity of the polymer because of higher charge density on the copolymer chains even though the microgels are dispersed in high salt concentration solution.[22,30] In addition, pNIPAm-based microgels show continuous changes in diameter below the VPTT.[31] As a result, microgels in the oxidized Ru^{III} state have larger hydrodynamic diameters at any temperature than those in the reduced Ru^{II} state.

Next, in order to clarify the differences of microgel properties between the Ru^{II} and the Ru^{III} states, we also checked the transmittance changes of NRu microgel dispersions as a function of temperature under the different conditions of the reduced Ru^{II} and the oxidized Ru^{III} states at high salt concentration (Figure 3). As can be seen from Figure 3a for NRu0.1(1) microgels, the transmittance curves almost coincided between in the Ru^{II} and the Ru^{III} states. Here the curves show cloud points at around LCST of pNIPAm in pure water.[14] On the other hand, the microgels having the oxidized Ru^{III} showed higher cloud points than those having the reduced Ru^{II} as shown in Figure 3b−f. Then the deviations of cloud points for each microgel increased with increasing immobilized $Ru(bpy)_3$

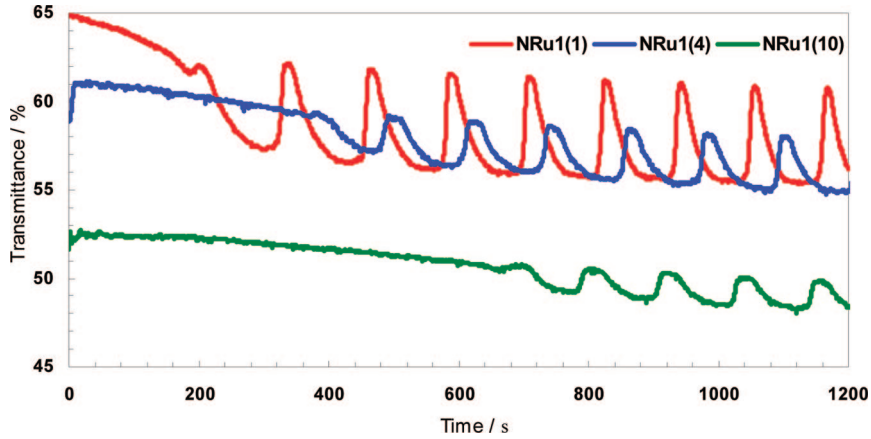

Figure 4. Self-oscillating profiles of optical transmittance for NRu1(1) (red line), NRu1(4) (blue line), and NRu1(10) microgels (green line). The microgels (100 μM of Ru(bpy)$_3$) were dispersed in aqueous solutions containing MA (62.5 mM), $NaBrO_3$ (84 mM), and HNO_3 (0.3 M) at 25 °C. Microgel concentration was 0.25 wt % in all cases.

Table 2. Cloud Points and Critical Flocculation Temperatures (CFTs) of the Ru(bpy)$_3$ Copolymerized PNIPAm Microgels

	cloud point, °C		CFT, °C	
sample	Ru^{II} state	Ru^{III} state	Ru^{II} state	Ru^{III} state
NRu0.1(1)	33.5	33.7	33	33
NRu0.2(1)	33.0	33.8	33	33
NRu0.5(1)	33.1	33.9	32	34
NRu1(1)	32.6	35.5	32	34
NRu1(4)	32.9	34.9	32	34
NRu1(10)	33.6	35.7	33	35

amounts in the microgels. Note that control experiment using the microgels dispersed in pure water suggested that large transmittance changes at cloud points reflect the microgel flocculation for all samples shown in Figure 3 (see Supporting Information).

Table 2 summarizes CFTs and cloud points measured in this study. It is clear to mention that CFTs correspond to cloud points for all microgels in both the reduced Ru^{II} and the oxidized Ru^{III} states although there are small differences in values due to the different microgel concentrations and characterization methods. This indicates that the microgels flocculate when they are heated up to their cloud points (i.e., LCSTs) of the microgels. These deviations in hydrodynamic diameters and different colloidal stabilities between in the Ru^{II} and the Ru^{III} states at the same temperature would result in self-oscillation of the microgels.

Investigation of Microgel Self-Oscillation. We carried out the BZ reaction using the NRu microgels. Here MA (62.5 mM), $NaBrO_3$ (84 mM), and HNO_3 (0.3 M) were used as substrates for the BZ reaction at fixed concentrations for all experiments. As can be expected from the results shown in Figures 2 and 3, the microgels having less Ru(bpy)$_3$ did not show strong volume oscillation (see Supporting Information). So herein, we used NRu1(1), NRu1(4), and NRu1(10) microgels [i.e., they were synthesized using the same amount of Ru(bpy)$_3$ monomer but the different amount of cross-linker] to clarify the volume oscillation of microgels, especially the effect of immobilization of metal catalyst for the BZ reaction into cross-linked hydrogel particles. Figure 4 shows the typical oscillation profiles of transmittance for the three different NRu microgel dispersions. For all profiles, the oscillations were observed after an induction period, which is a typical phenomenon of the BZ reaction. In addition, oscillation periods and amplitudes of transmittance change should be the indicators for the oscillations. Because the BZ reaction is sensitive to temperature, stirring, and initial concentrations of substrates (i.e., [MA], [$NaBrO_3$], [HNO_3]), we cannot explain the characteristics of the microgel self-oscillation clearly only from this data shown in Figure 4. So, we conducted further investigations by changing temperatures while the other conditions were fixed (i.e., initial concentrations of substrates, stirring, and microgel concentrations).

Figure 5 shows the oscillation profiles of transmittance for NRu1(10) microgel dispersions as a function of temperature. At low temperatures (15−28 °C), the amplitude of the oscillation became slightly bigger on raising the temperature (e.g., 1.4% at 15 °C and 2.2% at 28 °C). The increase in amplitude is mainly

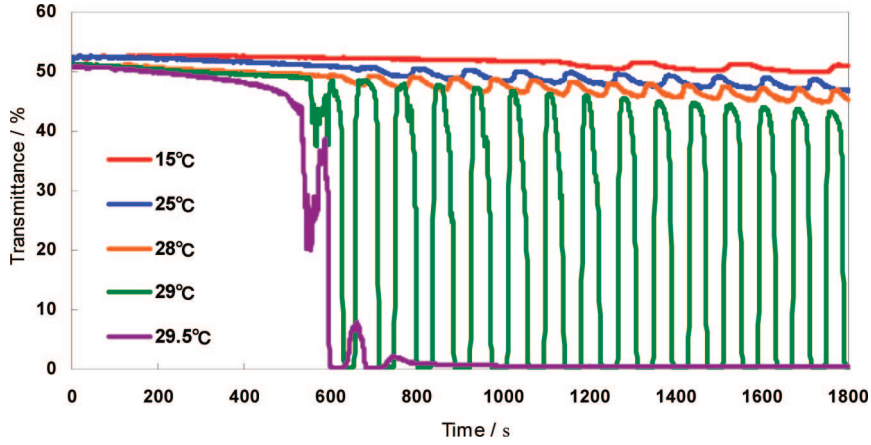

Figure 5. Self-oscillating profiles of optical transmittance for NRu1(10) microgel dispersions. The microgels (100 μM of Ru(bpy)$_3$) were dispersed in aqueous solutions containing MA (62.5 mM), $NaBrO_3$ (84 mM), and HNO_3 (0.3 M). The profiles were measured at the different temperatures: 15 °C (red line), 25 °C (blue line), 28 °C (orange line), 29 °C (green line), and 29.5 °C (purple line).

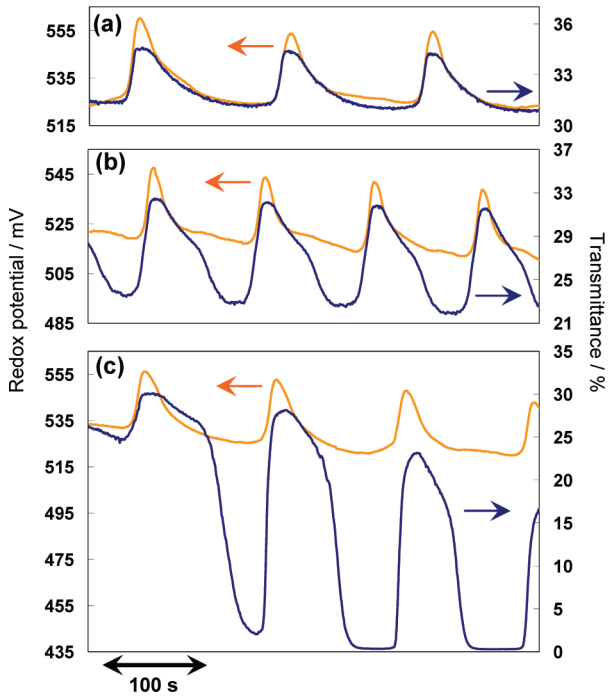

Figure 6. Simultaneous measurements of redox potential (orange line) and transmittance (blue line) of self-oscillation using NRu1(1) microgels. The microgels (100 μM of Ru(bpy)$_3$) were dispersed in aqueous solutions containing MA (62.5 mM), $NaBrO_3$ (84 mM), and HNO_3 (0.3 M) under the different temperatures: 25 °C (a), 27 °C (b), and 27.5 °C (c).

due to increased deviation of the hydrodynamic diameter between in the Ru^{II} and Ru^{III} states, as shown in Figure 2. This tendency was found clearly when less cross-linked microgels were used (i.e., NRu1(1) and NRu1(4) microgels; see Supporting Information and ref 19). Between 28 and 29 °C, remarkable changes in waveform and amplitude were observed. Then only 0.5 °C increase (i.e., at 29.5 °C) led to decrease the amplitude of the oscillations dramatically, and the periodic transmittance changes could no longer be observed at the higher temperatures (data not shown). Our previous work suggested that the dramatic change in oscillation waveform and amplitude is related to the difference in colloidal stability between in the Ru^{II} and the Ru^{III} states.[19]

In order to explain the two different oscillations around the VPTT (i.e., volume oscillation and flocculating/dispersing oscillation), we compared optical transmittance changes of microgels with redox potential change of the BZ reaction. Figure 6 shows three representative waveforms of transmittance changes observed from simultaneous measurements of the redox potential and transmittance changes. As can be clearly seen from Figure 6a, the transmittance curve corresponds well to the redox potential curve at 25 °C. This means that microgel volume oscillations are synchronized with the chemical reactions of the BZ reaction, which was also observed from our previous work using the bulk gels.[32] In contrast, the transmittance curve does not correspond to the redox potential curve at 27 and 27.5 °C due to the flocculating/dispersing oscillation of microgels. Here, dramatic transmittance decreases of the microgel oscillation were observed when the microgels were in the reduced Ru^{II} state. Taking the CFT deviations between in the Ru^{II} and the Ru^{III} states (see Figure 2) into consideration, these waveform changes of the transmittance are reasonable, thus due to the microgel flocculations.

Next, we compared microgel oscillations with the bulk solution of the BZ reaction in terms of the induction period. Figure 7 shows induction periods for the microgel oscillations

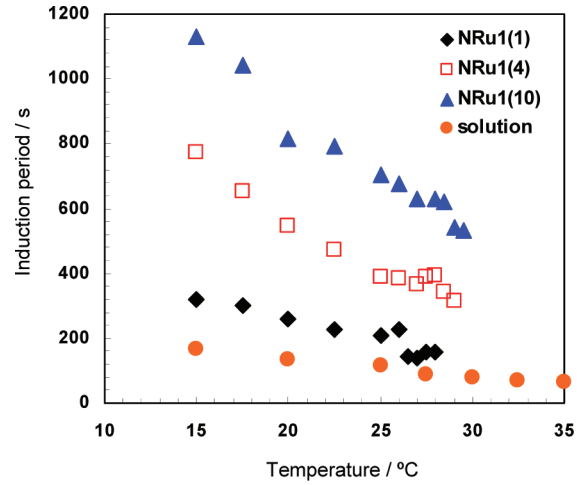

Figure 7. Effect of temperature and cross-linked density of microgels on the duration of the induction period. The microgels (100 μM Ru(bpy)$_3$) were dispersed in aqueous solutions containing MA (62.5 mM), $NaBrO_3$ (84 mM), and HNO_3 (0.3 M). Samples are NRu1(1) (black diamond), NRu1(4) (red square), NRu1(10) (blue triangle), and bulk solution (orange circle).

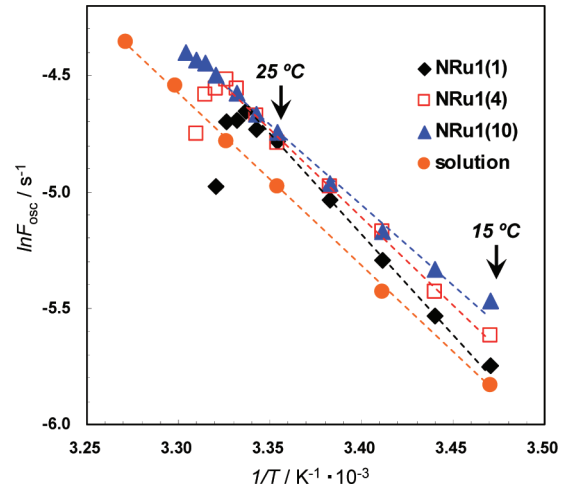

Figure 8. Arrhenius dependence of oscillation frequency (F_{osc}) using NRu1(1) (black diamond), NRu1(4) (red square), and NRu1(10) microgels (blue triangle). The microgels (100 μM Ru(bpy)$_3$) were dispersed in aqueous solutions containing MA (62.5 mM), $NaBrO_3$ (84 mM), and HNO_3 (0.3 M). Control experiments of the BZ reaction without microgel were investigated (orange circle) in the same aqueous solution.

and the bulk solution as a function of temperature. Note that induction periods for the microgel systems could not be measured above the VPTTs of the microgels due to microgel flocculation. Induction period for the microgel systems became longer than that for the conventional BZ reaction at all temperatures. Moreover, induction period became much longer at all temperatures as the cross-linked density of microgels increased. The most accepted hypothesis to explain the induction period of the BZ reaction is that crucial concentration of the organic brominated species, mainly bromomalonic acid (BrMA), must be reached before oscillation begins.[33] So, the results shown in Figure 7 can be understood by the effect of Ru(bpy)$_3$ immobilization in microgels, which is similar to gel-immobilized enzyme reaction.[34] In microgel systems studied here, the rate of BrMA production should be lower than that for the bulk solution due to lower diffusion constant of substrates and intermediates in microgels.

We also compared microgel oscillations with the conventional BZ reaction in terms of the oscillation period, P_{osc}. In this study,

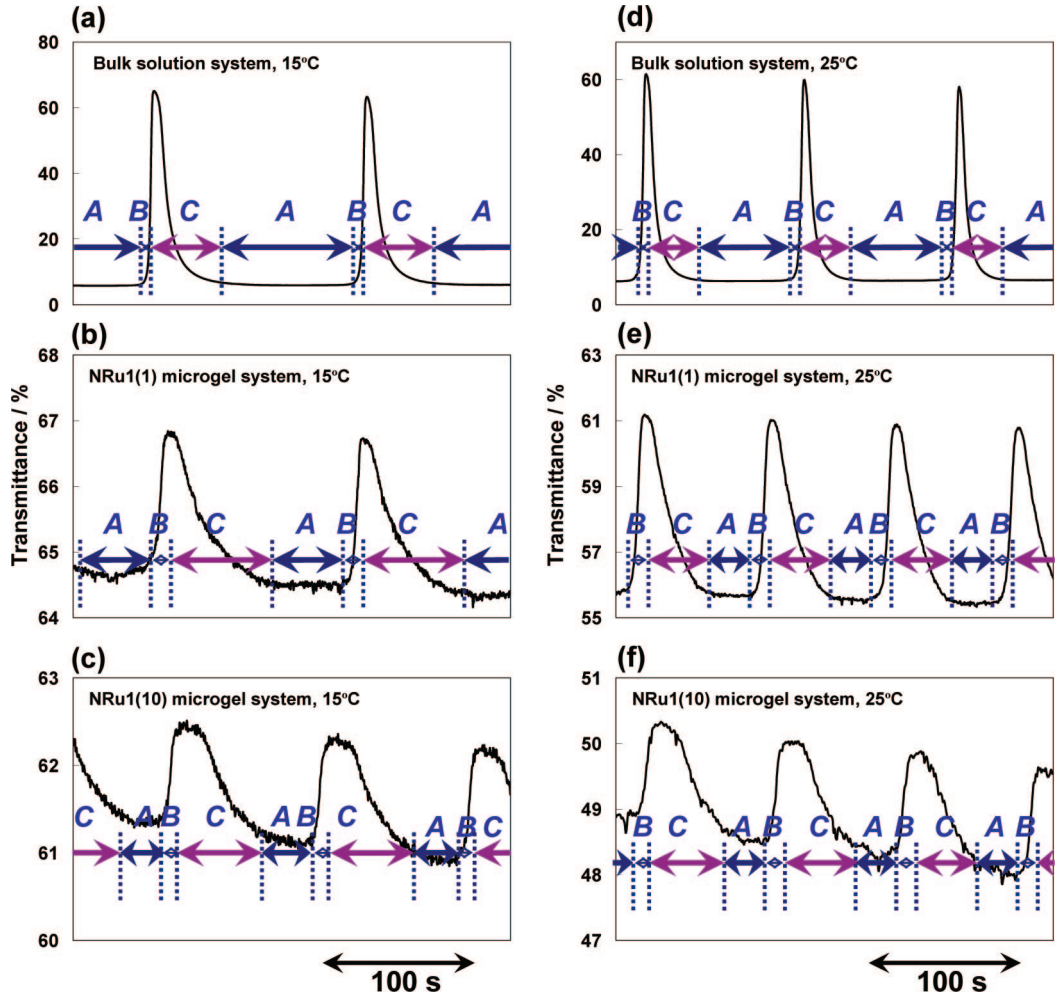

Figure 9. Typical oscillation waveforms in bulk solution (a, e), NRu1(1) (b, f), NRu1(4) (c, g), and NRu1(10) microgels (d, h). The microgels (100 μM of Ru(bpy)$_3$) were dispersed in the aqueous solutions containing MA (62.5 mM), $NaBrO_3$ (84 mM), and HNO_3 (0.3 M). The profiles were measured at the different temperatures: 15 °C (a−d) and 25 °C (e−h).

the average value of the period between the second and the sixth oscillation was regarded as the oscillation period. Since our measurements of oscillations were completed while a few percent of the initial quantity of the substrates were consumed, concentration of the substrate at a certain measuring time may be approximated to its initial concentration. Here the oscillation frequency, F_{osc} ($F_{osc} = 1/P_{osc}$), was used for analysis. As shown in Figure 8, the oscillation frequency of the bulk solution tends to increase as the temperature increases, in accordance with the Arrhenius equation.[35] In all microgel systems studied here, the Arrhenius equation could be adapted below the VPTT, as shown in Figure 8. On the other hand, the oscillation frequency decreases around the VPTTs due to the flocculating/dispersing oscillation, and the corresponding plots deviated from the Arrhenius equation. These deviations may be related to the lowered diffusibility of substrates and intermediates in the highly deswollen microgel aggregates; thus, the oscillation frequency decreased. In addition, it is clear to say that the oscillation frequency in microgel systems became higher than that in the bulk solution system. Moreover, the oscillation frequency became higher at low temperatures (e.g., 15 °C) as the cross-linked density of microgels increased, but the oscillation frequencies were almost equal at 25 °C, which is close to the VPTTs. These results for the microgel oscillation seem to be related to the different deswelling ratio for each microgel having different cross-linked densities; that is, gel network structures are looser as the cross-linked density of microgels decreases at 15 °C while they are almost equal at 25 °C (e.g., compare parts d−f of Figure 2). As a conclusion, we found that microgel structure plays an important role to control the oscillation frequency (= period). In addition, taking the gel network structure changes between in the Ru^{II} and the Ru^{III} states into consideration, not only the temperature and the microgel used but also the volume oscillation did affect the BZ reaction (i.e., feedback mechanism from mechanical to chemical change acts in the synchronization process).

To understand the effect of Ru(bpy)$_3$ immobilization in microgels on the oscillation period in detail, we compared the representative waveforms observed in the microgel systems and the bulk solution system (Figure 9). Before comparing these waveforms, we will provide the outline of the Field−Körös−Noyes (FKN) mechanism.[36] According to this scheme, the overall BZ reaction may be divided into the following three main processes: consumption of bromide ion (process A), autocatalytic reaction of bromous acid with oxidation of the catalyst (process B), and organic reaction with reduction of the catalyst (process C).

$$\text{A:}\quad BrO_3^- + 2Br^- + 3H^+ \rightarrow 3HOBr \tag{1}$$

$$\text{B:}\quad BrO_3^- + HBrO_2 + 2M_{red} + 3H^+ \rightarrow 2HBrO_2 + 2M_{ox} + H_2O \tag{2}$$

$$\text{C:}\quad 2M_{ox} + MA + BrMA \rightarrow fBr^- + 2M_{red} + \text{other products} \tag{3}$$

Following the FKN mechanism, we divided the waveforms into processes A, B, and C as shown in Figure 9. Table 3 summarizes

Table 3. A/P_{OSC}, B/P_{OSC}, and C/P_{OSC} Values for the Bulk Solution System and the Microgel Systems

sample	temp, °C	P_{osc}, s	A, s	B, s	C, s	A/P_{osc}	B/P_{osc}	C/P_{osc}
bulk solution	15	341	211	29	101	0.62	0.09	0.30
NRu1(1)	15	314	131	34	149	0.42	0.11	0.47
NRu1(10)	15	242	75	39	128	0.31	0.16	0.53
bulk solution	25	144	92	10	42	0.64	0.07	0.29
NRu1(1)	25	115	36	17	62	0.31	0.15	0.54
NRu1(10)	25	116	35	18	63	0.30	0.16	0.54

the oscillation periods P_{osc}, durations of processes A−C, and A/P_{osc}, B/P_{osc}, and C/P_{osc} values for the bulk solution system and the microgel systems. At the same temperatures, B/P_{osc} and C/P_{osc} values for the microgel systems became larger than that for the bulk solution system. Particularly, these values became larger as the cross-linked density of the microgels increased at 15 °C, but these values for the microgel systems were almost constant at 25 °C. The results can be also understood by the effect of $Ru(bpy)_3$ immobilization in microgels because processes B and C contain catalytic reaction; the rate of an immobilized catalytic reaction is lower than that of the same amount of soluble catalyst. In contrast, A/P_{osc} values for the microgel systems became smaller than that for the bulk solution system. And the values became smaller as the cross-linked density of the microgels increased at 15 °C, but the values for the microgel systems were almost constant at 25 °C. The smaller A/P_{osc} values for the microgel systems may be related to their larger C/P_{osc} values; that is, the lowered rate of process C affects process A. The details are currently under investigation by varying the initial concentrations of the substrates. As a result, we found that the changes of the oscillation period in the microgel systems are due to two contrastive effects: the smaller A/P_{osc} values and the larger B/P_{osc} and C/P_{osc} values, which resulted in the shorten oscillation period in this study as shown in Figure 8.

Conclusion

The self-oscillating microgels of NIPAm, $Ru(bpy)_3$ monomer, and cross-linker BIS have been synthesized by surfactant-free aqueous precipitation polymerization. In the polymerization, $Ru(bpy)_3$ monomer plays as stabilizers of the precursor particles, and microgel sizes became smaller, as confirmed by DLS. The volume oscillation of the microgels was detected by changes in optical transmittance. In particular, the flocculating/dispersing oscillation of the microgels was observed around the phase transition temperature, with a remarkable change in optical transmittance. The flocculating/dispersing oscillation of the microgels was also confirmed by comparing the optical transmittance changes of the microgels and the redox potential change of the BZ reaction. In order to analyze the microgel self-oscillation in detail, three characteristics (induction period, oscillation period, and waveform) of the microgel oscillation were compared with those of the bulk solution BZ reaction. Because of the effect of catalyst immobilization in microgels on the BZ reaction, induction time became longer than that for the bulk solution; however, the oscillation periods became shorter. The latter can be well explained by dividing the waveforms into three main processes followed by the FKN mechanism. These results suggest that not only energy transformation from chemical to mechanical change but also feedback mechanism from mechanical to chemical change acts in the synchronization process. Through the analysis in this paper, we found that temporal structure resulting from interparticle interaction among the microgels can be controlled by designing static network structure of the microgels on the basis of chemical synthetic procedure, differently from the previous paper in which only the phenomenon was demonstrated.[19] This finding would be important for future developments such as microgel assembly and controlled release.

Acknowledgment. D.S. is grateful to the research fellowships of the Japan Society for the Promotion of Science for Young Scientists. We are grateful to Dr. Masanori Ueda for useful discussion on electrochemical measurement.

Supporting Information Available: Absorption spectra for $Ru(bpy)_3$ monomer (SI Figure 1); temperature dependence of optical transmittance for microgels in pure water (SI Figure 2), in different $[NaBrO_3]$ solutions (SI Figure 3), at different microgel dispersion concentrations (SI Figure 4); self-oscillating profiles of optical transmittance for NRu0.1(1), NRu0.2(1), NRu0.5(1), and control NRu0(1) microgels (SI Figure 5); self-oscillating profiles of optical transmittance for NRu1(4) microgel dispersions (SI Figure 6); typical self-oscillating profiles of optical transmittance for many hours (SI Figure 7). This material is available free of charge via the Internet at http://pubs.acs.org.

References and Notes

(1) Hsiue, G. H.; Hsu, S. H.; Yang, C. C.; Lee, S. H.; Yang, I. K. *Biomaterials* **2002**, *23*, 457–462.
(2) Nayak, S.; Lee, H.; Chmielewski, J.; Lyon, L. A. *J. Am. Chem. Soc.* **2004**, *126*, 10258–10259.
(3) (a) Suzuki, D.; Kawaguchi, H. *Langmuir* **2005**, *21*, 8175–8179. (b) Suzuki, D.; Kawaguchi, H. *Langmuir* **2005**, *21*, 12016–12024. (c) Suzuki, D.; Kawaguchi, H. *Langmuir* **2006**, *22*, 3818–3822. (d) Suzuki, D.; Kawaguchi, H. *Colloid Polym. Sci.* **2006**, *284*, 1443–1451.
(4) (a) Zhang, J.; Xu, S.; Kumacheva, E. *J. Am. Chem. Soc.* **2004**, *126*, 7908–7914. (b) Zhang, J.; Xu, S.; Kumacheva, E. *Adv. Mater.* **2005**, *17*, 2336–2340.
(5) (a) Lu, Y.; Mei, Y.; Ballauff, M.; Drechsler, M. *J. Phys. Chem. B* **2006**, *110*, 3930–3937. (b) Lu, Y.; Mei, Y.; Drechsler, M.; Ballauff, M. *Angew. Chem., Int. Ed.* **2006**, *45*, 813–816.
(6) (a) Morris, G. E.; Vincent, B.; Snowden, M. J. *J. Colloid Interface Sci.* **1997**, *190*, 198–205. (b) Kawaguchi, H.; Kisara, K.; Takahashi, T.; Achiha, K.; Yasui, M.; Fujimoto, K. *Macromol. Symp.* **2000**, *151*, 591–598.
(7) Fujii, S.; Read, E. S.; Binks, B. P.; Armes, S. P. *Adv. Mater.* **2005**, *17*, 1014–1018.
(8) Suzuki, D.; Tsuji, S.; Kawaguchi, H. *J. Am. Chem. Soc.* **2007**, *129*, 8088–8089.
(9) (a) Weissman, J. M.; Sunkara, H. B.; Tse, A. S.; Asher, S. A. *Science* **1996**, *274*, 959–960. (b) Reese, C. E.; Mikhonin, A. V.; Kamenjicki, M.; Tikhonov, A.; Asher, S. A. *J. Am. Chem. Soc.* **2004**, *126*, 1493–1496.
(10) (a) Suzuki, D.; McGrath, J. G.; Kawaguchi, H.; Lyon, L. A. *J. Phys. Chem. C* **2007**, *111*, 5667–5672. (b) Lyon, L. A.; Debord, J. D.; Debord, S. B.; Jones, C. D.; McGrath, J. G.; Serpe, M. J. *J. Phys. Chem. B* **2004**, *108*, 19099–19108.
(11) Tsuji, S.; Kawaguchi, H. *Langmuir* **2005**, *21*, 8439–8442.
(12) Hu, Z.; Lu, X.; Gao, J. *Adv. Mater.* **2001**, *13*, 1708–1712.
(13) (a) Serpe, M. J.; Kim, J.; Lyon, L. A. *Adv. Mater.* **2004**, *16*, 184–187. (b) Kim, J.; Serpe, M. J.; Lyon, L. A. *J. Am. Chem. Soc.* **2004**, *126*, 9512–9513. (c) Kim, J.; Serpe, M. J.; Lyon, L. A. *Angew. Chem., Int. Ed.* **2005**, *44*, 1333–1336.
(14) (a) Heskins, M.; Guillet, J. E. *J. Macromol. Sci., Chem.* **1968**, *A2*, 1441–1455. (b) Schild, H. G. *Prog. Polym. Sci.* **1992**, *17*, 163–249.
(15) (a) Pelton, R. *Adv. Colloid Interface Sci.* **2000**, *85*, 1–33. (b) Nayak, S.; Lyon, L. A. *Angew. Chem., Int. Ed.* **2005**, *44*, 7686–7708.
(16) Ito, S.; Ogawa, K.; Suzuki, H.; Wang, B. L.; Yoshida, R.; Kokufuta, E. *Langmuir* **1999**, *15*, 4289–4294.
(17) (a) Sershen, S. R.; Westcott, S. L.; Halas, N. J.; West, J. L. *J. Biomed. Mater. Res.* **2000**, *51*, 293–298. (b) Nayak, S.; Lyon, L. A. *Chem. Mater.* **2004**, *16*, 2623–2627.
(18) Kim, J.; Nayak, S.; Lyon, L. A. *J. Am. Chem. Soc.* **2005**, *127*, 9588–9592.
(19) Suzuki, D.; Sakai, T.; Yoshida, R. *Angew. Chem., Int. Ed.* **2008**, *47*, 917–920.
(20) Zaikin, A. N.; Zhabotin, A. M. *Nature (London)* **1970**, *225*, 535–537.
(21) Maeda, S.; Hara, Y.; Sakai, T.; Yoshida, R.; Hashimoto, S. *Adv. Mater.* **2007**, *19*, 3480–3484.
(22) Yoshida, R.; Takahashi, T.; Yamaguchi, T.; Ichijo, H. *J. Am. Chem. Soc.* **1996**, *118*, 5134–5135.
(23) Ghosh, P. K.; Spiro, T. G. *J. Am. Chem. Soc.* **1980**, *102*, 5543–5549.
(24) International Standard ISO13321, 1996. Methods for determination of particle size distribution part 8. International Organization for Standardization (ISO).
(25) Kaszuba, M.; McKnight, D.; Connah, M. T.; McNeil-Watson, F. K.; Nobbmann, U. *J. Nanopart. Res.* **2008**, *10*, 823–829.

(26) Ueda, M.; Hara, Y.; Sakai, T.; Yoshida, R.; Takai, M.; Ito, Y. *J. Polym. Sci., Part B: Polym. Phys.* **2007**, *45*, 1578–1588.
(27) Wu, X.; Pelton, R. H.; Hamielec, A. E.; Woods, D. R.; McPhee, W. *Colloid Polym. Sci.* **1994**, *272*, 467–477.
(28) McPhee, W.; Tam, K. C.; Pelton, R. *J. Colloid Interface Sci.* **1993**, *156*, 24–30.
(29) Fernández-Nieves, A.; Fernández-Barbero, A.; Vincent, B.; de las Nieves, F. J. *Macromolecules* **2000**, *33*, 2114–2118.
(30) Yoshida, R.; Sakai, T.; Ito, S.; Yamaguchi, T. *J. Am. Chem. Soc.* **2002**, *124*, 8095–8098.
(31) Wu, C.; Zhou, S. *Macromolecules* **1997**, *30*, 574–576.
(32) Yoshida, R.; Tanaka, M.; Onodera, S.; Yamaguchi, T.; Kokufuta, E. *J. Phys. Chem. A* **2000**, *104*, 7549–7555.
(33) Sirimungkala, A.; Forsterling, H. D.; Dlask, V.; Field, R. J. *J. Phys. Chem. A* **1999**, *103*, 1038–1043.
(34) Kokufuta, E. *Prog. Polym. Sci.* **1992**, *17*, 647–697.
(35) Ruoff, P. *Physica D* **1995**, *84*, 204–211.
(36) (a) Field, R. J.; Körös, E.; Noyes, R. M. *J. Am. Chem. Soc.* **1972**, *94*, 8649–8664. (b) Field, R. J.; Noyes, R. M. *J. Chem. Phys.* **1974**, *60*, 1877–1884.

MA800684D